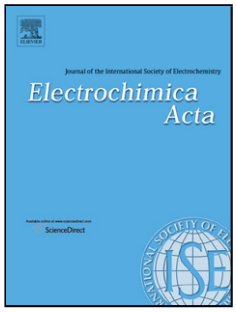

Title: Phosphate ions as corrosion inhibitors for reinforcement steel in chloride-rich environments

Author: L. Yohai M. Vázquez M.B. Valcarce<ce:footnote id="fn0005"><ce:note-para id="npar0005">ISE active member.</ce:note-para></ce:footnote>

PII: S0013-4686(13)00619-1
DOI: http://dx.doi.org/doi:10.1016/j.electacta.2013.03.180
Reference: EA 20289

To appear in: *Electrochimica Acta*

Received date: 21-12-2012
Revised date: 26-3-2013
Accepted date: 27-3-2013

Please cite this article as: L. Yohai, M. Vázquez, M.B. Valcarce, Phosphate ions as corrosion inhibitors for reinforcement steel in chloride-rich environments, *Electrochimica Acta* (2013), http://dx.doi.org/10.1016/j.electacta.2013.03.180

Phosphate ions as corrosion inhibitors for reinforcement steel in chloride-rich environments

L. Yohai, M. Vázquez[* 1] and M. B. Valcarce[1]

División Electroquímica y Corrosión,

Facultad de Ingeniería, Universidad Nacional de Mar del Plata – INTEMA, CONICET,

J. B. Justo 4302, B7608FDQ Mar del Plata, ARGENTINA

March 25, 2013

1 ISE active member

* corresponding author

División Electroquímica y Corrosión, Facultad de Ingeniería, Universidad Nacional de Mar del Plata, INTEMA, CONICET

Juan B. Justo 4302 - B7608FDQ Mar del Plata – Argentina

e-mail: mvazquez@fi.mdp.edu.ar

Tel.: +54 223 481 6600 ext 244, Fax : +54 223 481 0046

Abstract

Phosphate ions were evaluated as corrosion inhibitors in solutions that simulate the composition of the pores in concrete contaminated with chloride ions. Cyclic voltammograms and potentiodynamic polarization tests were complemented with micro-Raman spectroscopy and impedance spectroscopy to follow the performance of this inhibitor. Long term performance involved weight loss evaluation. Chloride contamination increases the accumulation of corrosion products on the metallic surface and promotes pitting corrosion. In contrast, pitting is inhibited when phosphate ions are incorporated in a 1:1 phosphate to chloride molar ratio, even after a 90 days exposure. Micro Raman spectra clearly show the incorporation of phosphates to the passive film. Impedance spectroscopy results can be interpreted assuming a duplex surface film formed in the presence of phosphates. In the conditions of this investigation, phosphate ions behave as mixed-type corrosion inhibitors, protecting steel against corrosion in chloride-contaminated environments.

Key words: phosphate; inhibitors; chloride; steel; concrete

1. Introduction

Reinforced concrete is one of the most widely used building materials. However, aggressive service environments and contaminated aggregates can contribute to its early deterioration and failure. Steel corrosion is one of the main factors that negatively influences the overall performance of reinforced concrete.

The durability of reinforced concrete structures is partially explained by the high alkalinity of concrete (pH can easily attain values close to 12 – 13), which results in the formation of a passive layer on the steel rebar. This is the reference situation simulated by our experiments in the pore simulating solution (PSS). As long as the integrity of this passive film is guaranteed, the corrosion rate will be minimal [1].

The composition, structure and morphology of the surface film controls rebar corrosion rates. Even though the behavior of carbon steel corrosion has been studied comprehensively [2-4], uncertainties related to film formation and deterioration mechanisms still persist. As the literature shows, surface film formation and degradation vary considerably with the composition of the electrolyte (pH, additives, oxygen content, aggressive anions and others), temperature and surface pretreatments. So, given the wide variety of service conditions that can be expected, it is difficult to determine how the corrosion process will evolve.

The two most common causes of rebar corrosion are (i) localized breakdown of the passive film on the steel due to penetration of chloride ions [5, 6] and (ii) generalized corrosion by acidification of the concrete after reaction with atmospheric carbon dioxide [7-9]. Even worse is the combination of these two factors. When a structure is located in a marine environment, chloride ions can penetrate the porous structure of concrete and reach the steel. On top of this, in many coastal cities in Argentina, the use of

seasand and chloride-contaminated coarse aggregates and water constitutes a recurrent malpractice [10].

To minimize the effect of rebar corrosion, various techniques are frequently employed, such as cathodic protection, inhibitors dosage or the application of coatings to the external concrete surface or to the reinforcing steel bars. The use of corrosion inhibitors is considered as one of the most cost-effective solutions. Damage can be prevented by adding the corrosion inhibitor to the concrete mixture or by treating the rebars prior to building the structure. Chromate, phosphate, nitrite, tungstate and molybdate ions have been investigated in terms of their ability to inhibit the pitting corrosion of steel [9, 11-13].

Compared to alternative inhibiting agents, phosphates present some advantages such as low cost and low toxicity. Some authors consider that phosphates are anodic inhibitors, being effective only in the presence of oxygen [14-16]. Other authors suggest that they act as cathodic inhibitors for $[PO_4^{-3}]/[Cl^-]$ ratios lower than 0.6 while they behave as mixed inhibitors for $[PO_4^{-3}]/[Cl^-]$ ratios higher than 0.6 [17, 18]. Few articles have reported evaluations of the inhibitor performance of phosphate ions in simulated concrete solutions [13, 14, 19, 20]. The action mechanism of this agent in highly alkaline solutions needs to be clarified to later evaluate its effectiveness in mortars. In this work, the effectiveness of sodium phosphate (0.3 mol dm^{-3}) as corrosion inhibitor has been tested in a synthetic medium (pH 13) that simulates the interstitial solution of concrete contaminated with chlorides. The composition of the passive films in the presence of the contaminant and the inhibitor are investigated, so that a protection mechanism can be proposed.

2. Materials and methods

2.1. Electrodes preparation

The electrodes were constructed from steel reinforcement bars (Mn 0.635 wt%, C 0.299 wt%, Si 0.258 wt%, Cu 0.227 wt% and others impurities 0.245 wt%). Disc samples of steel were included in fast curing epoxy resin on appropriated polyvinyl chloride (PVC) holders. The geometrical area exposed was 0.503 cm^2. An electrical contact was prepared at the back of each sample. The electrodes were abraded down to grade 1000 with emery paper. The electrodes were then rinsed gently with distilled water.

2.2. Electrolyte composition

The experiments were carried out using a pore simulating solution (PSS). The composition was KOH 0.08 mol dm^{-3}, NaOH 0.02 mol dm^{-3} and $Ca(OH)_2$ 0.001 mol dm^{-3} with a resulting pH value of 13. When chloride ions were incorporated, the Cl^- dosage used was 0.3 mol dm^{-3} corresponding to $[Cl^-]/[OH^-]=3$. These solutions are labelled as PSS + Cl^-. To evaluate the inhibitor effect, the dosage of Na_3PO_4 tested was 0.3 mol dm^{-3}, corresponding to $[PO_4^{3-}]/[Cl^-]=1$. These solutions will be referred to as PSS + Cl^- + PO_4^{3-}. All the experiments were carried out at room temperature (20 ± 2 ºC).

2.3. Electrochemical techniques

All the electrochemical experiments were performed in a three-electrode cell. A Voltalab PGZ 100 potentiostat was used. A Hg/HgO electrode with 1 mol dm^{-3} KOH solution (labeled as MOE, E = 0.123 V vs. SHE) was used as reference. All the

potentials are indicated against this electrode. The counter electrode was a platinum wire of large area.

The corrosion potential (E_{corr}) was measured during 24 h in the different conditions investigated. Average values of at least five individual experiments were registered. Potentiodynamic polarization tests were also executed after having kept the electrodes for 24 h at E_{corr}.

Cyclic voltammograms were recorded after having deaerated the electrolyte by bubbling N_2 during 15 min prior to each measurement. The electrodes were pre-reduced in PSS at –1.1 V_{MOE}. Finally the scan was started at −1.1 V_{MOE} and reversed at convenient values. The sweep rate used was 10 mV s^{-1}.

Film growth was investigated carrying out polarization tests in deareated PSS applying a potentiodynamic scan of 1 mV s^{-1}. The starting point was the positive potential where the oxide had been grown. The potential was scanned in the negative direction up to –1.15 V_{MOE}.

For the anodic polarization curves, the potentiodynamic scan started at the E_{corr}, with a sweep rate of 0.1 mV s^{-1}. The scan direction was reversed when reaching 100 μA cm^{-2}. This value was chosen to induce a convenient degree of attack. The overall procedure followed the recommendations of ASTM [21].

Electrochemical impedance spectroscopy (EIS) tests were performed at open circuit potential, after having kept the electrodes for 24 h at E_{corr} in the testing solutions, without stirring or deaereating. The amplitude of the AC applied potential signal was ± 0.01 Vrms while the frequency varied between 20 kHz and 1 mHz. The results were analyzed using two different equivalent circuits presented in Figure 1. The circuit **a** is typical of oxide-coated metals [9, 12, 22, 23]. The circuit **b** presents an additional

Warburg element that could be attributed to a diffusion process [24, 25]. The experimental data were fitted to the proposed equivalent circuit using ZView™ [26].

2.4. Ex-situ Raman spectra

The Raman measurements were carried out using an Invia Reflex confocal Raman microprobe with Ar^+ laser of 514 nm in backscattering mode, with a laser spot of 10 μm. An exposure time of 50 s and 3 accumulations were used, with 50 X objective. The laser power was 25 mW. Raman spectra were collected on least five representative spots after having subjected the electrodes to anodic polarization curves. The spectra were observed to be reproducible.

2.5. Weight loss determinations

The weight loss method was applied following the guidelines in ASTM D 2688 Standard Test Methods for Corrosivity of Water in the Absence of Heat Transfer. Coupons, in the shape of disks having 5.67 cm^2 as geometrical area, were cut and abraded down to grade 120 with emery paper. Previously weighted coupons were suspended and immersed in the following test solutions: PSS, PSS + Cl^- and PSS + Cl^- + PO_4^{3-}. Each container held three coupons. The containers were kept at room temperature in aerated conditions. The coupons were withdrawn after 90 days. For surface characterization, one coupon of each condition was conveniently dried to perform *ex-situ* Raman spectra. Then the corrosion products were stripped by immersion in HCl 1 mol dm^{-3}. Later the coupons were neutralized and rinsed, first with a saturated Na_2CO_3 solution and then with distilled water, to be finally dried and reweighted.

3. Results and discussion

Figure 2 shows the first cycle of voltammograms carried out in PSS, PSS + Cl^- and PSS + Cl^- + PO_4^{3-}. In PSS, four peaks can be seen in the positive scan, in agreement with the results obtained by other authors [27-30]. The first anodic peak at -0.92 V_{MOE} (Ia) has been attributed before to the oxidation of atomic hydrogen absorbed into the metal during the cathodic pre-reduction process. Then, peak IIa at -0.74 V_{MOE} can be attributed to the formation of hydrated Fe(II) and Fe(III) species and eventually Fe_3O_4. At pH 13, the solubility of Fe(II) species is minimal and that of Fe(III) is maximal [28]. Peak IIIa at -0.6 V_{MOE} could be attributed to the formation of $Fe(OH)_3$ and/or α- or δ-FeOOH by oxidation of Fe(II) compounds formed at IIa, such as Fe_3O_4. This process takes place at the film solution interface, leading to the generation of cation vacancies [28]. The formation of δ-FeOOH at pH = 14 has been demonstrated before using Raman spectroscopy [27]. Peak IVa at -0.30 V_{MOE} has been suggested to comprise the conversion of $Fe(OH)_2$ to an Fe(III) hydroxide or oxyhydroxide different from those formed at IIIa, such as $Fe(OH)_3$ or γ-FeOOH [28]. In PSS, at potentials positive to that of peak IVa, the positive end of the potential sweep may be extended up to 0.6 V_{MOE} without any further current increment. After reversing the scan, two cathodic peaks can be seen in PSS. Peak Ic at -0.69 V_{MOE} can be attributed to the reduction of Fe(III) species and peak IIc at -0.89 V_{MOE} to that of Fe(II) species. As can be seen, the total cathodic charge is lower than the anodic charge. This has been attributed before to the fact that once a magnetite-like phase forms, further $Fe(OH)_2$ dissolution will be limited since magnetite is quite insoluble and known to inhibit iron dissolution [28]. The presence of magnetite at highly cathodic potential has been verified experimentally

before, using in situ Raman spectroscopy [30]. This work also shows that the surface film presents a layered structure in which the inner part is Fe_3O_4 within most of the potential range examined, while the outer part is oxidized or reduced depending on the applied potential.

When chloride ions are added, the scan needs to be reverted at more negative potentials to avoid localized attack. In PSS + Cl^- , the same four oxidation peaks can be seen in Figure 2. As iron is readily oxidized when in contact with chloride ions, the intensity of peaks IIa and IIIa increases markedly. In this chloride-rich electrolyte, only one reduction peak is clearly seen. This can be due to the smaller potential window and also to the higher solubility of the iron oxides or hydroxides in the presence of chloride ions. This is in agreement with XPS results [31], which showed that the addition of chloride to the solution decreased the thickness of the oxide film and also changed the stoichiometry of surface film, such that near the film/metal interface the Fe^{3+}/Fe^{2+} ratio increased.

After incorporating phosphate ions to the electrolyte, the positive limit can again attain more positive values, as was the case for PSS. In PSS + Cl^- + PO_4^{3-}, the same oxidation peaks are found except for the one at -0.6 V_{MOE} (IIIa). Only one broad cathodic band from -0.6 to -1.0 V_{MOE} can be seen. There is insufficient information in the literature on the behavior of steel when chloride and phosphate ions are simultaneously present [13, 31-34], with almost no reference to the composition of the surface film. Even if the strong interaction between iron oxides and phosphate ions is clearly demonstrated, the actual role played by phosphate is still controversial. Both, the incorporation of iron phosphates to the surface film and the simple adsorption of phosphates on the surface have been given as plausible interpretations. The results from EIS and micro Raman spectroscopy, to be discussed below, will demonstrate that in the present case the

composition of the surface layer does change and that of phosphate ions incorporate to the passive film.

Figure 3a shows the tenth cycle of cyclic voltammograms in PSS, PSS + Cl^- and PSS + Cl^- + PO_4^{3-}. In every condition, the sweep was reverted at the same potential to allow an easier comparison of the anodic and cathodic charges. The presence of just one negative and one positive peak as the number of cycles in the voltammogram increases has been reported before [28, 29]. In PSS and PSS + Cl^- the charge related to both peaks increases steadily with each new cycle. This behavior, presented in Figure 3b for PSS + Cl^-, has also been observed previously by many authors [27, 28, 35]. This increment has been attributed to the accumulation of corrosion products on the steel surface (particularly the accumulation of a sublayer of magnetite which is never completely reduced), ultimately leading to a continuous thickening of the surface layer as more cycles are recorded. This is not the case when PO_4^{3-} ions are present: after ten cycles the anodic and cathodic charges are very similar to those in the first cycle. This behavior could be related to the absence of peak IIIa in Figure 2. If Fe(III) compounds are not being formed, they cannot be reduced and then formed again, on further cycle [27]. It has been argued that chloride ions induce dissolution and phosphate ions promote ferrous phosphate precipitation, given the higher solubility of ferric phosphate (pK_{sp} = 32 for ferrous phosphate compared to pK_{sp} = 26 for ferric phosphate) [36].

Figure 4 shows the potentiodynamic polarization curves on electrodes that had been kept for 24 h at the E_{corr} in PSS + Cl^- and PSS + Cl^- + PO_4^{3-}. E_{corr} values can be seen in Table 1. In order to improve the definition of the peaks, the scan rate of the potentiodynamic curves is 10 times lower than that of the cyclic voltammograms. Two peaks appear in the alkaline chloride-contaminated solution, one at -0.97 V_{MOE} and another at -0.82 V_{MOE}, in agreement with a film composed by Fe(II) and Fe(III)

oxohydroxydes [31, 37]. A quite different behavior was found when phosphates are present. There are no peaks, and the current increases steadily but with values always lower in magnitude than those in PSS + Cl^-, indicating the development of a thinner passive layer or one which is more difficult to reduce.

The impedance spectra recorded using electrodes aged during 24 hours in PSS + Cl^- with and without inhibitor, together with the fit results are shown in Figures 5a, b and c in the form of Nyquist and Bode plots. The fitting parameters are presented in Table 2.

Corroding electrodes may show various types of non-homogeneities, which can be represented using constant phase elements (CPE) instead of capacitors in the equivalent circuit. Surface roughness, deficient polishing, grain boundaries and surface impurities had been mentioned before among the main reasons that justify the use of CPEs in equivalent circuits that model corroding electrodes [38]. The impedance of this type of element is frequency-dependent, and can be defined using two parameters, Q and *n* as:

$$Z_{CPE} = [Q(j\omega)^n]^{-1} \quad (1)$$

where Q is a constant with dimensions of $\Omega\ cm^2\ s^{-(1-n)}$ and *n* a constant power, with $-1<n<1$. By plotting the imaginary component of the impedance as a function of frequency in a logarithmic scale has been used before to quantify the CPE behavior [39]. As shown in Figure 5d, a slope of -0.93 was obtained, in agreement with the n_o values presented in Table 2.

Warburg impedances and CPEs with a *n* value around 0.5 (the last known as "infinite diffusion") are used to model surface layers with increasing ionic conductivity due to corrosion processes occurring inside the pores, and the consequent diffusion process

along them. If the surface layer is thin, low frequencies will penetrate the entire thickness creating a finite length Warburg element (Eq. 2):

$$Zw = \frac{W_R}{(iT\omega)^n}\tanh(iT\omega)^n \qquad (2)$$

where W_R is a parameter associated with solid phase diffusion and T is related to the effective diffusion coefficient (D) and the effective diffusion thickness (L) by $T = L^2/D$. Only if the layer is thick enough so that the lowest frequencies are unable to penetrate the entire width, can its behavior be interpreted as infinite diffusion [26].

The experimental data fit reasonably to the equivalent circuits proposed in Figure 1. R_s represents the solution resistance, Q_o the pseudo-capacitance of the surface film, R_o the film resistance, Q_t the metal pseudo-capacitance, R_t the charge-transfer resistance for metal dissolution, and W represents a Warburg element associated to finite length diffusion through in the film.

In the absence of inhibitor, a depressed loop with two time constants in the Bode plot indicates the development of a surface layer, which in this case is the passive layer [9, 12, 40]. The spectra were fitted using the equivalent circuit in Figure 1 **a**. On the other hand, in the presence of inhibitor, two loops in the Nyquist plot can be observed, one at high frequencies, and the other at low frequencies. The loop at low frequencies presents two time constants, so that a total of three times constants can be observed in the Bode plot in phosphate-containing electrolytes. In this condition, the results were fitted using the equivalent circuit in Figure 1 **b.**

When the inhibitor is incorporated, Q_o and n_o do not present significant changes when compared to a phosphate-free electrolyte, as shown in Table 2. The similar values of Q_o together with n_o values higher than 0.9 can be related to a capacitive response associated

to the presence of a protective passive layer [12, 28, 40]. However, R_o decreases markedly when the inhibitor is incorporated. This decrease could be associated to two factors: to an increment in the porosity of the surface film [25] or to changes in the composition of the surface film. In a more porous film an increment of Q_o should be observed as a result of water filling the pores, with a consequent decrease of n_o [41, 42]. However, this behavior is not observed. Therefore the decrease of R_o is probably related to changes in the composition which impact the electronic properties [28], instead of being associated to an increment in the porosity of the passive film. The Q_t value calculated for the low frequency loop is too high to be associated with a double layer capacitance. This Q_t value is therefore associated with diffusion impedance combined with a charge transfer process [17]. Moreover, the low frequency loop exhibits an angle θ with respect to the real axis that approaches 45° as the frequency increases, which is in agreement with a diffusion process [43]. In the present case, the diffusion impedance could represent the hindered diffusion of oxygen through a non-conducting layer, where oxygen reduction only occurs after O_2 reaches the metal/film interfase. On the other hand, the diffusion impedance could be associated to a more difficult movement of cation vacancies. These vacancies are generated by chloride ions adsorption and diffuse from the film/solution interface across the film, towards the film/metal interface. If diffusion is slowed down, the vacancies condensate cannot reach the critical size at the film/metal interface, preventing pitting [44-46]. Along the same line, the slight increment in the R_t values in the presence of phosphate ions could be explained as the result of changes in composition which influence the electronic properties of the surface layers and could, in turn, affect the mass transfer of oxygen and/or cation vacancies.

The sequence of anodic polarization curves shown in Figure 6 was carried out in PSS, PSS + Cl^- and PSS + Cl^- + PO_4^{3-}. Steel remained passive in PSS. However, in the

presence of chloride ions, pitting occurred at potentials around 0.02 V_{MOE} and repassivation was not possible. The influence of Cl^- ions on the passivity breakdown of steel can be interpreted as a balance between two processes competing on the metal surface: stabilization of the passive film by OH^- adsorption and disruption of the film by Cl^- adsorption. When the activity of chlorides overcomes that of hydroxyls, pitting occurs [12]. When both phosphates and chloride ions are present in solution, pitting is clearly inhibited. Some relevant electrochemical parameters such as passivity currents (i_{pas}), corrosion potential (E_{corr}) and pitting potentials (E_{pit}) were calculated from at least six anodic polarization curves. These average results are presented in Table 1. As it can be seen, the beneficial effect of phosphates is clear: i_{pas} measured for PSS + Cl^- is nearly twice the i_{pas} measured in presence of the inhibitor. The role of phosphate ions as inhibiting agents has been explained before in terms of their strong interaction with iron oxo-hydroxides present in the passive film. By adsorbing on the surface, they can promote precipitation of dissolved iron species leading to iron phosphates, since these compounds are known to have very low solubility values [34]. It should be noticed that E_{corr} moved towards more negative values when Cl^- + PO_4^{3-} were present in the solution. This tendency has been observed previously by other authors [17, 18]. At high [PO_4^{3-}]/[Cl^-] ratios such as 1, phosphate acts as an mixed inhibitor, whereas at smaller ratios, phosphate becomes a cathodic inhibitor [17]. Micrographies of the steel surface were taken after anodic polarization experiments and are presented in Figure 7. The images confirm the absence of attack when phosphate ions are present.

Raman spectroscopy provides direct information on the bonding, composition and stoichiometry of both crystalline and amorphous surface compounds on metals, at atmospheric pressures. Ex-situ Raman spectra were registered in order to characterize the passive films and the corrosion products after inducing the pitting process by anodic

polarization. The results should be interpreted with caution because this technique may demand a relatively high laser power, given that the most common iron oxides and oxyhydroxides are poor light scatters [47]. In Figure 7, the arrows point to the regions where Raman spectra were collected (zone A in PSS + Cl^- + PO_4^{3-} and; zones B and C in PSS + Cl^- without and with corrosion products). The corresponding Raman spectra are presented in Figure 8. It has to be taken into account that laser irradiation may produce local heating effects which have been shown before to broaden the bands and induce shifts to lower wavenumbers [47]. Raman spectrum B corresponds to a region with no pitting attack, where there are no corrosion products present. In this condition, there is no evidence of defined peaks. This lack of characteristic signals may be due to the presence of a very thin passive film on the steel surface. Also, iron oxides or oxohydroxides could be forming an amorphous or disordered structure, obstructing a clear identification [32]. Raman spectrum C corresponds to a corroded region. The bands at 220 cm^{-1}, 280 cm^{-1}, 395 cm^{-1} and 595 cm^{-1} are typical of α-FeOOH [27, 32, 40]. Raman spectrum A shows a peak at 245 cm^{-1} that can be attributed to γ-FeOOH [32]. Also, Fe_3O_4 is present in the passive film showing its characteristic peak at 680 cm^{-1} [27, 32]. Phosphate ions have been reported to have four active Raman bands: an intense one at 935 cm^{-1} due to P-O symmetric stretch and three weak ones at 1007 cm^{-1} (P-O antisymmetric) and 550 and 412 cm^{-1} (deformation) [48]. Thus, the bands that can be seen at 940 and 1005 cm^{-1} are attributed to the presence of iron phosphates in the passive layer [34]. The band at 1081 cm^{-1} can be attributed to an antisymmetric stretching mode of hydrogen phosphate [48].

To evaluate the performance of the inhibitor at longer times, 90 days weight-loss tests were carried out by immersing steel coupons in PSS, PSS + Cl^-, PSS + Cl^- + PO_4^{3-}. Figure 9 shows photographs of the coupons after 90 days of immersion in each

electrolyte, as indicated. The corrosion current density values (i_{corr}) were calculated from weight loss results using Faraday's law [49]

$$i_{corr} = \frac{mF}{Ateq} \quad (3)$$

where m is the mass lost, F is the Faraday constant, A is the exposed area, t is the exposure time and eq is the equivalent weight (Fe eq= 27.92 g/mol).

The percentage of inhibition was calculated using the following equation

$$\%\zeta = \left[1 - \frac{i_{\text{corr with inhibitor}}}{i_{\text{corr without inhibitor}}}\right] x100 \quad (4)$$

The results are shown in Table 3. The coupon immersed in PSS can be taken as the control specimen. In this condition, corrosion and weight loss are negligible and the steel coupons present i_{corr} values typical of steel in passive state [50, 51]. As presented in Figure 9, no attack was detected in the case of coupons immersed in PSS + Cl^- + PO_4^{3-}. Also, the i_{corr} values are typical of the passive state, even when the samples have been immersed during 90 days. In contrast, pitting is evident in the case of coupons immersed in PSS + Cl^-.

The *ex-situ* Raman spectra of the corrosion products on the coupons are presented in Figure 10. The results obtained after 90 days are in agreement with those presented in Figure 8 after performing the anodic polarization curves. In the presence of the inhibitor, the composition of the passive layer changed and the participation of PO_4^{3-} is evident.

In summary, when carbon steel is exposed to aerated PSS + Cl^- at E_{corr}, the passive layer comprises mainly an inner layer of Fe_3O_4 with a lower density and more defective outer layer mostly composed of FeOOH [27, 28, 52]. After a long period of time at E_{corr}, the ratio Fe^{3+}/Fe^{2+} increases from the outer to the inner region creating cation vacancies and stress in the surface layer, leading to disruption [28]. This process is fast in the presence of chloride ions [31].

When carbon steel is exposed to PSS + Cl^- + PO_4^{-3} the first step in the surface layer formation could be related to the precipitation of ferrous phosphate by a dissolution-precipitation mechanism [36]:

$$3\ Fe + 2\ PO_4^{-3} \rightarrow (Fe)_3(PO_4)_2 + 6\ e^- \qquad (5)$$

Underneath this ferrous phosphate layer, a protective passive film of Fe_3O_4 could be formed via solid-state process [28]. This type of duplex passive film has been proposed by other authors when PO_4^{3-} ions are present in acidic or neutral media [53], and in phosphate buffer at pH = 8.4 [54]. Ferrous phosphate could be oxidized to ferric phosphate by reaction with oxygen [54]. After long periods of time at E_{corr} , the ferric phosphate layer could inhibit Fe_3O_4 oxidation, avoiding attack by chloride ions. Fe_3O_4 is a good conductor [30, 43], it is quite insoluble and known to inhibit iron dissolution [27-29]. In addition, this phosphate layer could delay oxygen diffusion through the duplex interface, hindering the consumption of the electrons produced by the anodic reaction taking place at the metal-film interface [43, 54].

Finally, it is worth noting that extrapolation to the behavior of steel embedded in mortar or concrete requires further investigation, currently in progress.

4. Conclusions

A synthetic solution that simulates the electrolyte contained in the pores of concrete contaminated with chlorides has been used to evaluate the performance of phosphate ions as corrosion inhibitors. The composition of the passive films on construction steel changes significantly in the presence of both, the contaminant and the inhibitor, either present individually o simultaneously. The addition of 0.3 mol dm^{-3} of chloride ions to the electrolyte promotes the accumulation of corrosion products on the metallic surface, changes the composition of the surface film and ultimately leads to pitting corrosion. Pits can be induced by anodic polarization or long term exposures.

When phosphate ions are incorporated ($[PO_4^{3-}]/[Cl^-]=1$) pitting is inhibited even if E_{corr} moves towards slightly more negative values. Even after 90 days at open circuit potential weight loss is minimal. The composition of the surface layer changes and micro Raman spectra clearly show the incorporation of phosphates to the passive film. In this condition (PSS + Cl^- + PO_4^{-3}) a duplex film is likely to be formed. This would consist of an outer layer of ferrous phosphate progressively oxidized to ferric phosphate, and an inner, protective layer of Fe_3O_4 formed via solid-state process. The outer layer is a poor conductor while Fe_3O_4 is a good conductor. The outer phosphate layer could delay oxygen diffusion, hindering further oxidation at the metal-film interface. This interpretation is supported by EIS results and ultimately leads to classify phosphate ions as a mixed-type inhibitor.

Figure captions

Figure 1. Equivalent circuits used to fit EIS results. Circuit **a** is typical of oxide-coated metals; circuit **b** presents an additional Warburg element, typical of situations where diffusion processes are involved.

Figure 2. Cyclic voltammograms for steel in PSS (──), PSS + Cl^-(─□─), PSS + Cl^- + PO_4^{3-} (─○─). Scan rate: 10 mV s^{-1}.

Figure 3. a) Cyclic voltammograms for steel (tenth cycle) in PSS (──), PSS + Cl^- (─□─), PSS + Cl^- + PO_4^{3-} (─○─); b) Cyclic voltammograms for steel in PSS + Cl^-, cycles 1 to 10. Scan rate: 10 mV s^{-1}.

Figure 4. Potentiodynamic curves on steel electrodes held 24 h at E_{corr} in PSS + Cl^- (─□─), PSS + Cl^- + PO_4^{3-} (─○─). Scan rate: 1 mV s^{-1}.

Figure 5. Impedance spectra recorded on steel electrodes aged during 24 hours at E_{corr} in SSP + Cl^- with and without inhibitor. The symbols represent the data and the lines the fitting results. (a) Nyquist representation; (b) and (c) Bode representation; (d) imaginary part of impedance as function of frequency, in logarithmic scale. PSS + Cl^-(─□─), PSS + Cl^- + PO_4^{3-} (─○─);

Figure 6. Anodic polarization curves of steel after being 24 h at E_{corr} in PSS (──), PSS + Cl^- (─□─), PSS + Cl^- + PO_4^{3-} (─○─). Scan rate: 0.1 mV s^{-1}.

Figure 7. Micrographs of the electrodes after having carried out anodic polarization curves. The arrows point the zones where Raman spectra were registered. Zone A in PSS + Cl^- + PO_4^{3-} and zones B and C in PSS + Cl^- without and with corrosion products.

Figure 8. Raman spectra of the steel surface after having carried out anodic polarization curves. Zone A (─○─) in PSS + Cl^- + PO_4^{-3} and zones B (──) and C (─□─) in PSS + Cl^- without and with corrosion products.

Figure 9. Photographs of the coupons after a 90 days period of immersion in PSS, PSS + Cl^-, PSS + Cl^- + PO_4^{3-}. Coupons diameter = 1.7 cm.

Figure 10. E*x-situ* Raman spectra from the coupons presented in Figure 9. PSS (—), PSS + Cl^-(—□—), PSS + Cl^- + PO_4^{3-} (—○—).

References

[1] K. Tuuti, Corrosion of Steel in Concrete, Sweedish Cement and Concrete Research Institute, 1982.

[2] D.W. Hobbs, Concrete deterioration: Causes, diagnosis, and minimising risk, Int. Mater. Rev. 46 (2001) 117-144.

[3] V. Kumar, Protection of steel reinforcement for concrete - A review, Corros. Rev. 16 (1998) 317-358.

[4] C.L. Page, K.W.J. Treadaway, Aspects of the electrochemistry of steel in concrete, Nature 297 (1982) 109-115.

[5] M.F. Montemor, A.M.P. Simões, M.G.S. Ferreira, Chloride-induced corrosion on reinforcing steel: From the fundamentals to the monitoring techniques, Cem. Con. Comp. 25 (2003) 491-502.

[6] X. Shi, N. Xie, K. Fortune, J. Gong, Durability of steel reinforced concrete in chloride environments: An overview, Constr. Build. Mater. 30 (2012) 125-138.

[7] M. Moreno, W. Morris, M.G. Alvarez, G.S. Duffo, Corrosion of reinforcing steel in simulated concrete pore solutions effect of carbonation and chloride content, Corros. Sci. 46 (2004) 2681-2699.

[8] L.J. Parrott, Proc. Durability of Building Materials and Components. Fifth International Conference, Brighton, UK, 1990.

[9] M.B. Valcarce, M. Vázquez, Carbon steel passivity examined in solutions with a low degree of carbonation: The effect of chloride and nitrite ions, Mater. Chem. Phys. 115 (2009) 313-321.

[10] W. Morris, M. Vázquez, Corrosion of reinforced concrete exposed to marine environment, Corros. Rev. 20 (2002) 469-508.

[11] S. Refaey, S. S. A. El-Rehim, F. Taha, M. B. Saleh and R. A. Ahmed, Inhibition of chloride localized corrosion of mild steel by PO_4, CrO_4, MoO_4, and NO_2 anions, Appl. Surf. Sci. 158 (2000) 190 - 196.

[12] M.B. Valcarce, M. Vázquez, Carbon steel passivity examined in alkaline solutions: The effect of chloride and nitrite ions, Electrochim. Acta 53 (2008) 5007-5015.

[13] N. Etteyeb, L. Dhouibi, H. Takenouti, M.C. Alonso, E. Triki, Corrosion inhibition of carbon steel in alkaline chloride media by Na_3PO_4, Electrochim. Acta 52 (2007) 7506-7512.

[14] J.M.R. Génin, L. Dhouibi, P. Refait, M. Abdelmoula, E. Triki, Influence of phosphate on corrosion products of iron in chloride-polluted-concrete-simulating solutions: Ferrihydrite vs green rust, Corrosion 58 (2002) 467-478.

[15] M.J. Pryor, M. Cohen, The inhibition of corrosion of iron by some anodic inhibitors, J. Electrochem. Soc. 100 (1953) 203-215.

[16] A.M. Simoes, J. Torres, R. Picciochi, J.C.S. Fernandes, Corrosion inhibition at galvanized steel cut edges by phosphates pigments, Electrochim. Acta 54 (2009) 3957-3865.

[17] L. Dhouibi, E. Triki, M. Salta, P. Rodrigues, A. Raharinaivo, Studies on corrosion inhibition of steel reinforcement by phosphate and nitrite, Mater. Struct. 36 (2003) 530-540.

[18] T.A. Söylev, M.G. Richardson, Corrosion inhibitors for steel in concrete: state of the art report, Constr. Build. Mater. 22 (2008) 609-622.

[19] N. Etteyeb, M. Sanchez, L. Dhouibi, C. Alonso, C. Andrade, E. Triki, Corrosion protection of steel reinforcement by a pretreatment in phosphate solutions: Assessment of passivity by electrochemical techniques, Corros. Eng., Sci. Techn. 41 (2006) 336-341.

[20] N. Etteyeb, L. Dhouibi, M. Sanchez, C. Alonso, C. Andrade, E. Triki, Electrochemical study of corrosion inhibition of steel reinforcement in alkaline solutions containing phosphates based components, J. Mater. Sci. 42 (2007) 4721-4730.

[21] American Society of Testing and Materials, ASTM G61-86. Standard Test Method for Conducting Cyclic Potentiodynamic Polarization Measurements for Localized Corrosion Susceptibility of Iron-, Nickel-, or Cobalt-Based Alloys. Philadelphia, 1993.

[22] A. Palit, S. Pehkonen, Copper corrosion in distribution systems: evaluation of a homogeneous Cu_2O film and a natural corrosion scale as corrosion inhibitors, Corros. Sci. 42 (2000) 1801-1822.

[23] J. Shim, J. Kim, Copper corrosion in potable water distribution systems: influence of copper products on the corrosion behaviour, Mater. Let. 58 (2004) 2002-2006.

[24] C. Liu, Q. Bi, A. Leyland, A. Matthews, An electrochemical impedance spectroscopy study of the corrosion behaviour of PVD coated steels in 0.5 N NaCl aqueous solution: Part I. Establishment of equivalent circuits for EIS data modelling, Corros. Sci. 45 (2003) 1243-1256.

[25] C. Liu, Q. Bi, A. Leyland, A. Matthews, An electrochemical impedance spectroscopy study of the corrosion behavior of PVD coated steels in 0.5 N NaCl aqueous solution: Part II. EIS interpretation of corrossion behaviour, Corros. Sci. 45 (2003) 1257-1273.

[26] ZPlot for Windows Scribner Associates Inc., 1998.

[27] A. Hugot-Le Goff, J. Flis, N. Boucherit, S. Joiret, J. Wilinski, Use of Raman spectroscopy and rotating split ring disk electrode for identification of surface layers on iron in 1M NaOH, J. Electrochem. Soc. 137 (1990) 2684-2690.

[28] W. Xu, K. Daub, X. Zhang, J.J. Noel, D.W. Shoesmith, J.C. Wren, Oxide formation and conversion on carbon steel in mildly basic solutions, Electrochim. Acta 54 (2009) 5727-5738.

[29] H. Zhang and S. Park, Rotating ring-disk electrode and spectroelectrochemical studies on the oxidation of iron in alkaline solutions, J. Electrochem. Soc. 141 (1994) 718-724

[30] S. Joiret, M. Keddam, X.R. Novoa, M.C. Perez, C. Rangel and H. Takenouti, Use of EIS, ring-disk electrode, EQCM and Raman spectroscopy to study the film of oxides formed on iron in 1M NaOH, Cem. Con. Comp. 24 (2002) 7 - 15.

[31] P. Ghods, O.B. Isgor, J.R. Brown, F. Bensebaa, D. Kingston, XPS depth profiling study on the passive oxide film of carbon steel in saturated calcium hydroxide solution and the effect of chloride on the film properties, Appl. Surf. Sci. 257 (2011) 4669-4677.

[32] B. Diaz, S. Joiret, M. Keddam, X. R. Novoa, M. C. Perez and H. Takenouti, Passivity of iron in red mud's water solutions, Electrochim. Acta 49 (2004) 3039-3048.

[33] H.W. Song, V. Saraswathy, S. Muralidharan, C.H. Lee, K. Thangavel, Role of alkaline nitrites in the corrosion performance of steel in composite cements, J. Appl. Electrochem. 39 (2009) 15-22.

[34] M. Reffass, R. Sabot, M. Jeannin, C. Berziou, P. Refait, Effects of phosphate species on localised corrosion of steel in $NaHCO_3$ + NaCl electrolytes, Electrochim. Acta 54 (2009) 4389-4396.

[35] P. Schmuki, M. Buchler, S. Virtanen, H.S. Isaacs, M.P. Ryan, H. Bohni, Passivity of iron in alkaline solutions studied by in situ XANES and a laser reflection technique, J. Electrochem. Soc. 146 (1999) 2097-2102.

[36] G. Vatankhah, H. Menard, H. Brossad, Effect of sulfate and chloride ions on the electrochemical bahaviour of iron in aqueous phosphate solutions, J. Appl. Electrochem. 28 (1998) 99-1004.

[37] W.C. Baek, T. Kang, H.J. Sohn, Y.T. Kho, In situ surface enhanced Raman spectroscopic study on the effect of dissolved oxygen on the corrosion film on low carbon steel in 0.01 M NaCl solution, Electrochim. Acta 46 (2001) 2321-2325.

[38] L.J. Aljinovic, S. Gudic, M. Smith, Inhibition of CuNi10Fe corrosion in seawater by sodium-diethyl-dithiocarbamate: an electrochemical and analytical study, J. Appl. Electrochem 30 (2000) 973-979.

[39] J.B. Jorcin, M.E. Orazem, N. Pébére, B. Tribollet, CPE analysis by local electrochemical impedance spectroscopy, Electrochim. Acta 51 (2006) 1473-1479.

[40] M.V. Valcarce, C. Lopez, M. Vazquez, The Role of Chloride, Nitrite and Carbonate Ions on Carbon Steel Passivity Studied in Simulating Concrete Pore Solutions, J. Electrochem. Soc. 159 (2012) C244- C251.

[41] M.E. Folquer, S.B. Ribotta, S.G. Real, L.M. Gassa, Study of copper dissolution and passivation processes by electrochemical impedance spectroscopy, Corrosion 58 (2002) 240-247.

[42] M.J. Esplandiu, E.M. Patrito, V.A. Macagno, Characterization of hafnium anodic oxide films: an AC impedance investigation, Electrochim. Acta 40 (1995) 809-815.

[43] M. Sancy, Y. Gourbeyre, E.M.M. Sutter, B. Tribollet, Mechanism of corrosion of cast iron covered by aged corrosion products: Application of electrochemical impedance spectrometry, Corros. Sci. 52 (2010) 1222-1227.

[44] N. Sato, An overview on the passivity of metals, Corros. Sci. 31 (1990) 1-19.

[45] D.D. Macdonald, Point defect model for the passive state, J. Electrochem. Soc. 139 (1992) 3434-3449.

[46] Y.F. Cheng, J.L. Luo, Electronic structure and pitting susceptibility of passive film on carbon steel, Electrochim. Acta 44 (1999) 2947-2957.

[47] D.L.A. de Faria, S. Venancio Silva, M.T. de Oliveira, Raman Microspectroscopy of Some Iron Oxides and Oxyhydroxides, J. Raman Spectrosc. 28 (1997) 873-878.

[48] S. Simard, M. Odziemkowski, D.E. Irish, L. Brossard, H. Ménard, In situ micro-Raman spectroscopy toinvestigate pitting corrosion product of 1024 mild steel in phosphate and bicarbonate solutions containing chloride and sulfate ions, J. Appl. Electrochem. 31 (2001) 913-920.

[49] American Society of Testing and Materials, ASTM G102-89, Standard Practice for Calculation of Corrosion Rates and Related Information from Electrochemical Measurements. Philadelphia, 1994.

[50] J.A. Gonzalez, E. Ramirez, A. Bautista, S. Feliu, The behaviour of pre-rusted steel in concrete, Cem. Con. Res. 26 (1996) 501-511.

[51] A. Poursaee, C.M. Hansson, Reinforcing steel passivation in mortar and pore solution, Cement & Concrete Research 37 (2007) 1127-1133.

[52] N. Sato, Toward a more fundamental understanding of corrosion processes, Corrosion 45 (1989) 354-368.

[53] I.V. Sieber, H. Hildebrand, S. Virtanem and P. Schmuki, Investigations on the passivity of iron in borate and phosphate buffers, pH 8.4, Corros. Sci. 48 (2006) 3472-3488.

[54] D.A. Jones, Principles and prevention of corrosion-2nd, Prentice-Hall Inc., 1996.

Table 1. Electrochemical parameters obtained from at least six anodic polarization curves for steel in the conditions evaluated.

	PSS	PSS + Cl^-	PSS + Cl^- + PO_4^{3-}
$[PO_4^{3-}]$ /mol dm^{-3}	------	------	0.3
$[Cl^-]$ /mol dm^{-3}	------	0.3	0.3
E_{corr} /mV_{MOE}	-208 ± 22	-237 ± 30	-263 ± 34
E_{pit} /mV_{MOE}	-----	6 ± 64	------
E_{pit}-E_{corr} /mV	------	182 ± 81	------
j_{pas} /μA cm^{-2}	0.7 ± 0.1	5.4 ± 2.6	0.9 ± 0.7

Table 2. Optimized parameters fitting data in Figs. 5 a, b and c to the equivalent circuits proposed in Fig.1.

	$[Cl^-]/[OH^-]=3$	
	PSS + Cl^-	PSS + Cl^- + PO_4^{3-}
$[PO_4^{3-}]$ /mol dm^{-3}	------	0.3
$[Cl^-]$ /mol dm^{-3}	0.3	0.3
R_s/Ω cm^2	6.20	4.27
$Q_o/\mu\Omega^{-1}$ cm^{-2}s^n	45.01	34.37
n_o	0.95	0.95
$R_o/k\Omega$ cm^2	55.06	0.18
$W_R/$ kΩ cm^2	------	0.57
T/s	------	1.81
n_W	------	0.32
$Q_t/\mu\Omega^{-1}$ cm^{-2} s^n	57.60	2141
n_t	0.61	0.67
$R_t/k\Omega$ cm^2	66.74	101.06

Table 3. Weight loss result after 90 days of immersion at E_{corr} in the different solutions tested.

	SSP	SSP + 0.3 mol dm^{-3} Cl^-	SSP + 0.3 mol dm^{-3} Cl^- + 0.3 mol dm^{-3} PO_4^{3-}
Weight loss/mg	0.1	221.2	0.3
Observation	Spotless surface	Pitting	Spotless surface
i_{corr}/μA cm^{-2}	0.006	14.0	0.02
% ξ	-----	-----	99.8

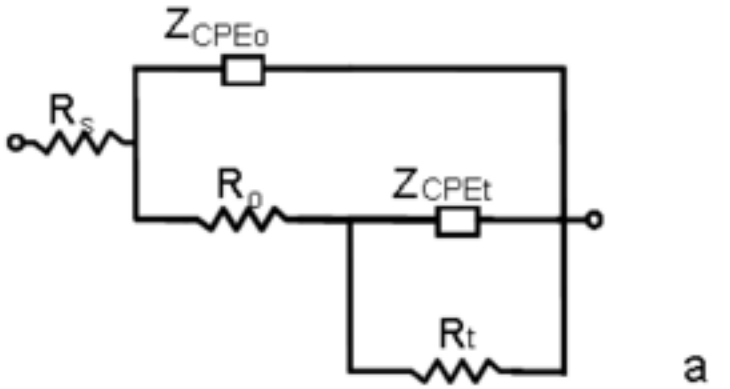

a

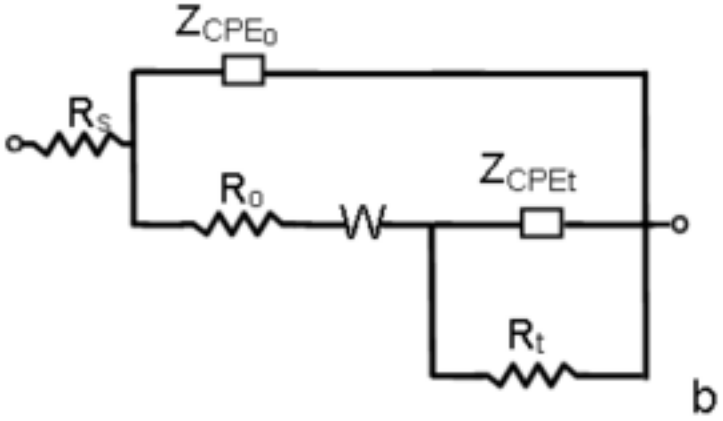

b

Figure 2

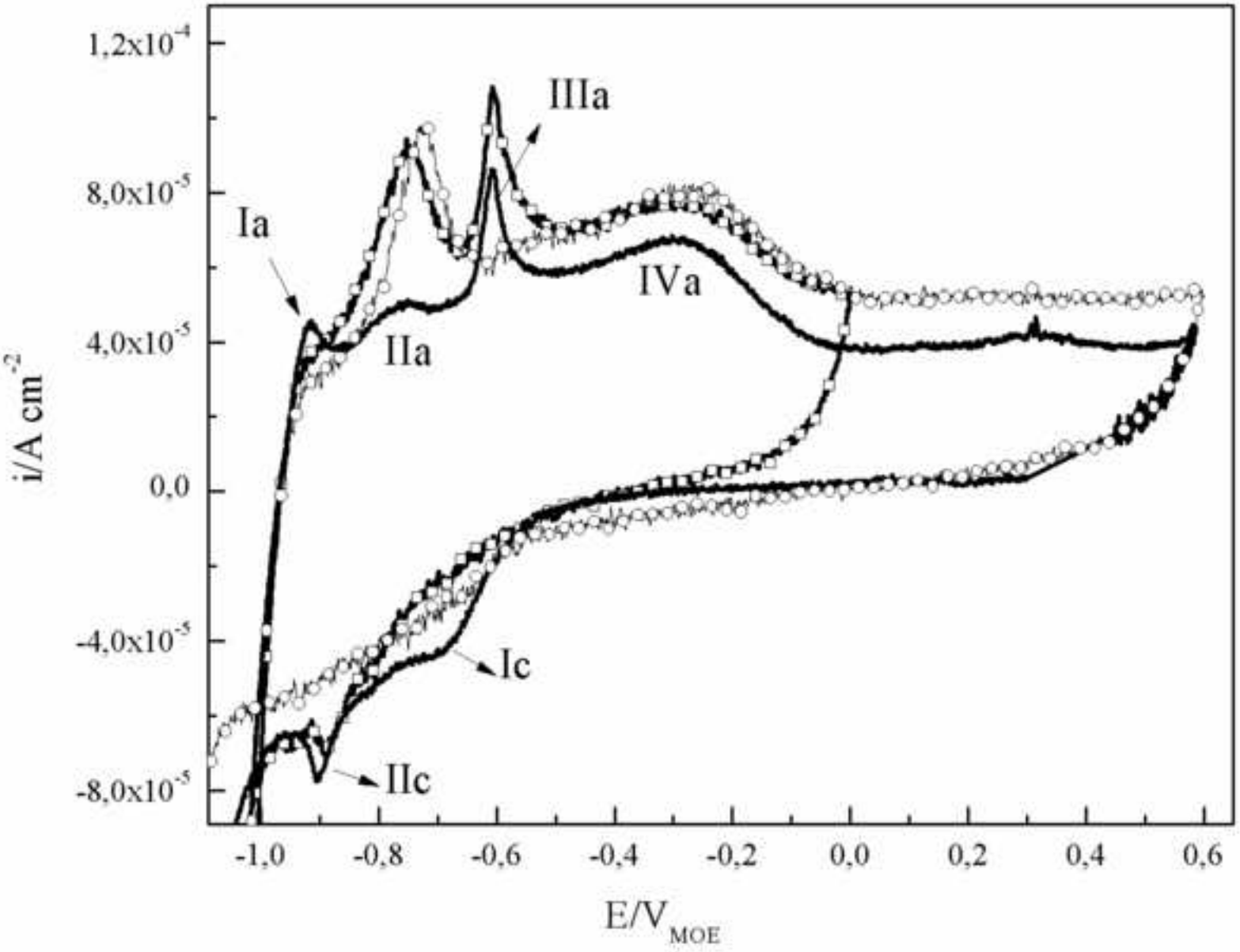
1,2x10-4
8,0x10-5
4,0x10-5
0,0
-4,0x10-5
-8,0x10-5
i/A cm-2
Ia
IIa
IIIa
IVa
Ic
IIc
-1,0
-0,8
-0,6
-0,4
-0,2
0,0
0,2
0,4
0,6
E/VMOE

Figure 3a

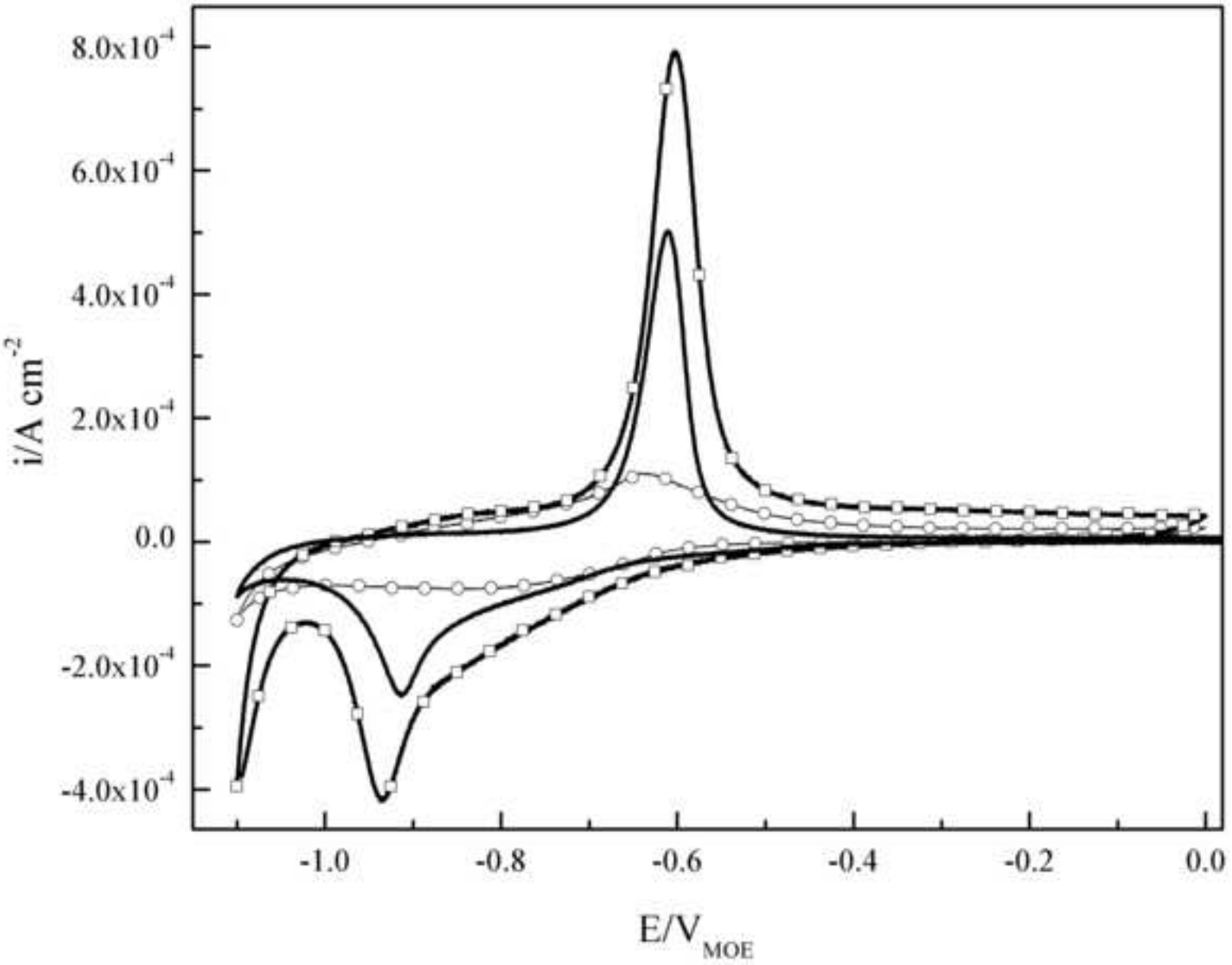
8.0x10-4
6.0x10-4
4.0x10-4
2.0x10-4
0.0
-2.0x10-4
-4.0x10-4
i/A cm-2
-1.0
-0.8
-0.6
-0.4
-0.2
0.0
E/VMOE

Figure 3b

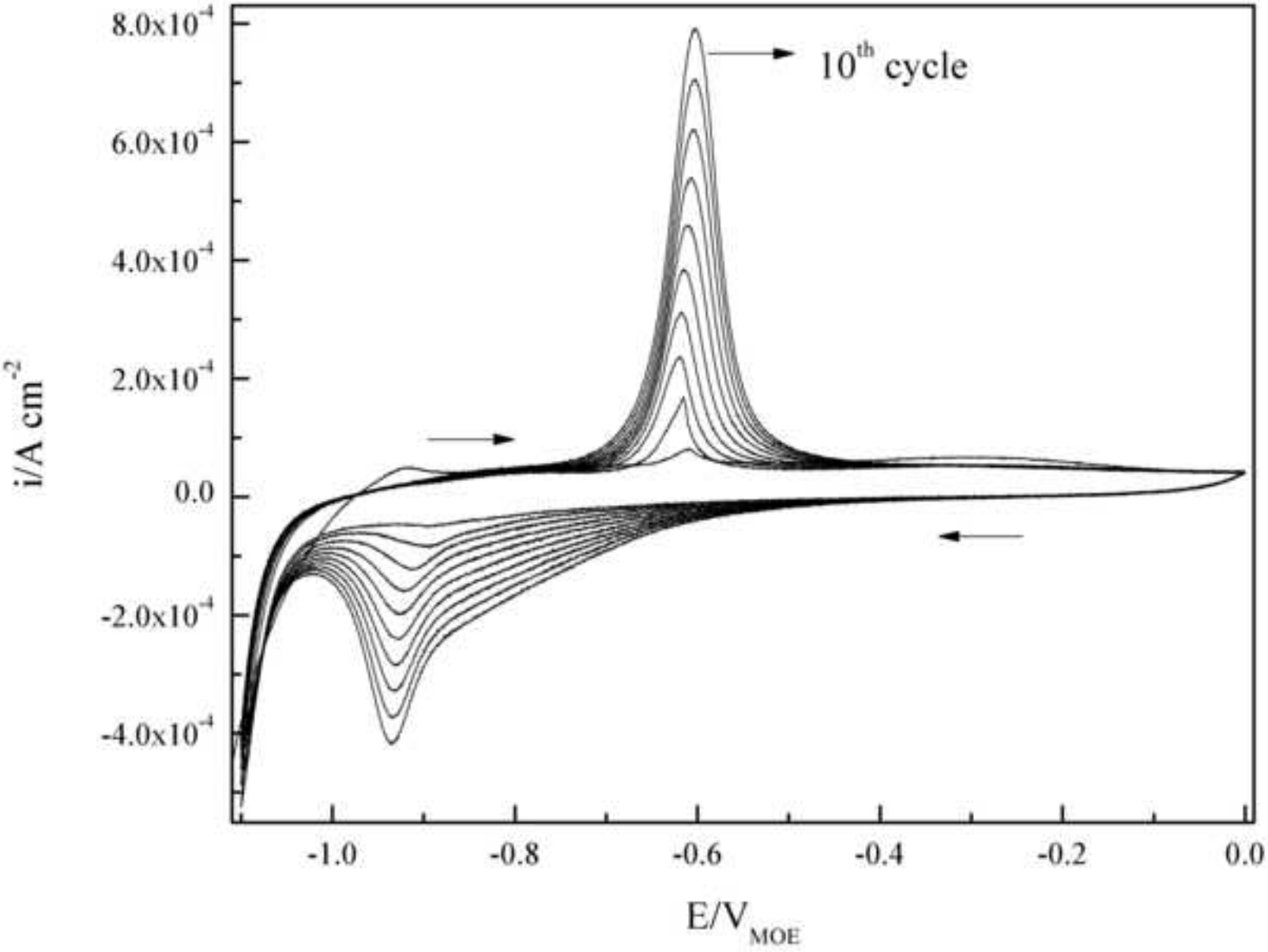
8.0x10-4
6.0x10-4
4.0x10-4
2.0x10-4
0.0
-2.0x10-4
-4.0x10-4
i/A cm-2
10th cycle
-1.0
-0.8
-0.6
-0.4
-0.2
0.0
E/VMOE

Figure 4

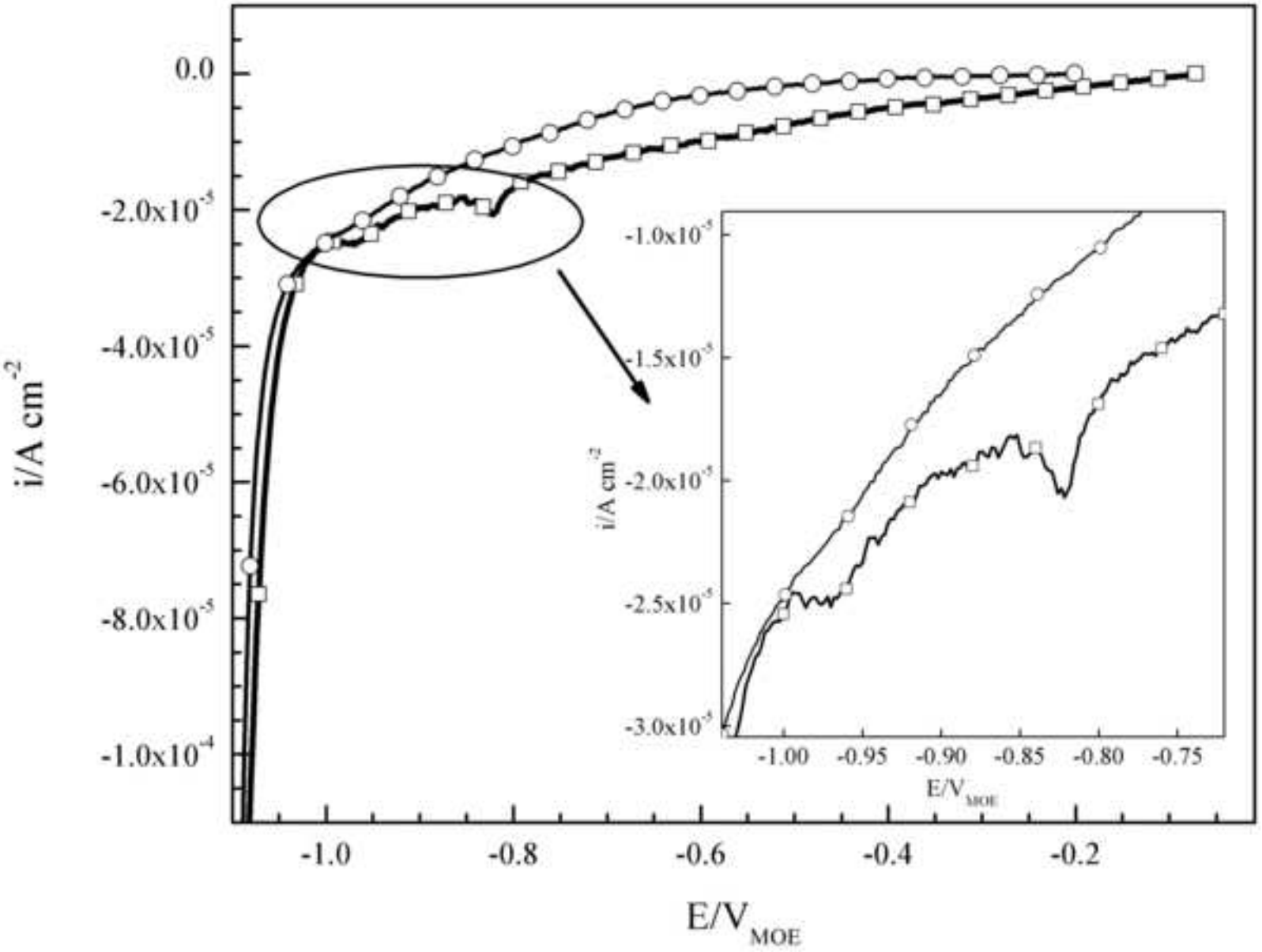
0.0
-2.0x10^-5
-4.0x10^-5
-6.0x10^-5
-8.0x10^-5
-1.0x10^-4
i/A cm^-2
-1.0
-0.8
-0.6
-0.4
-0.2
E/V_MOE
-1.0x10^-5
-1.5x10^-5
-2.0x10^-5
-2.5x10^-5
-3.0x10^-5
i/A cm^-2
-1.00
-0.95
-0.90
-0.85
-0.80
-0.75
E/V_MOE

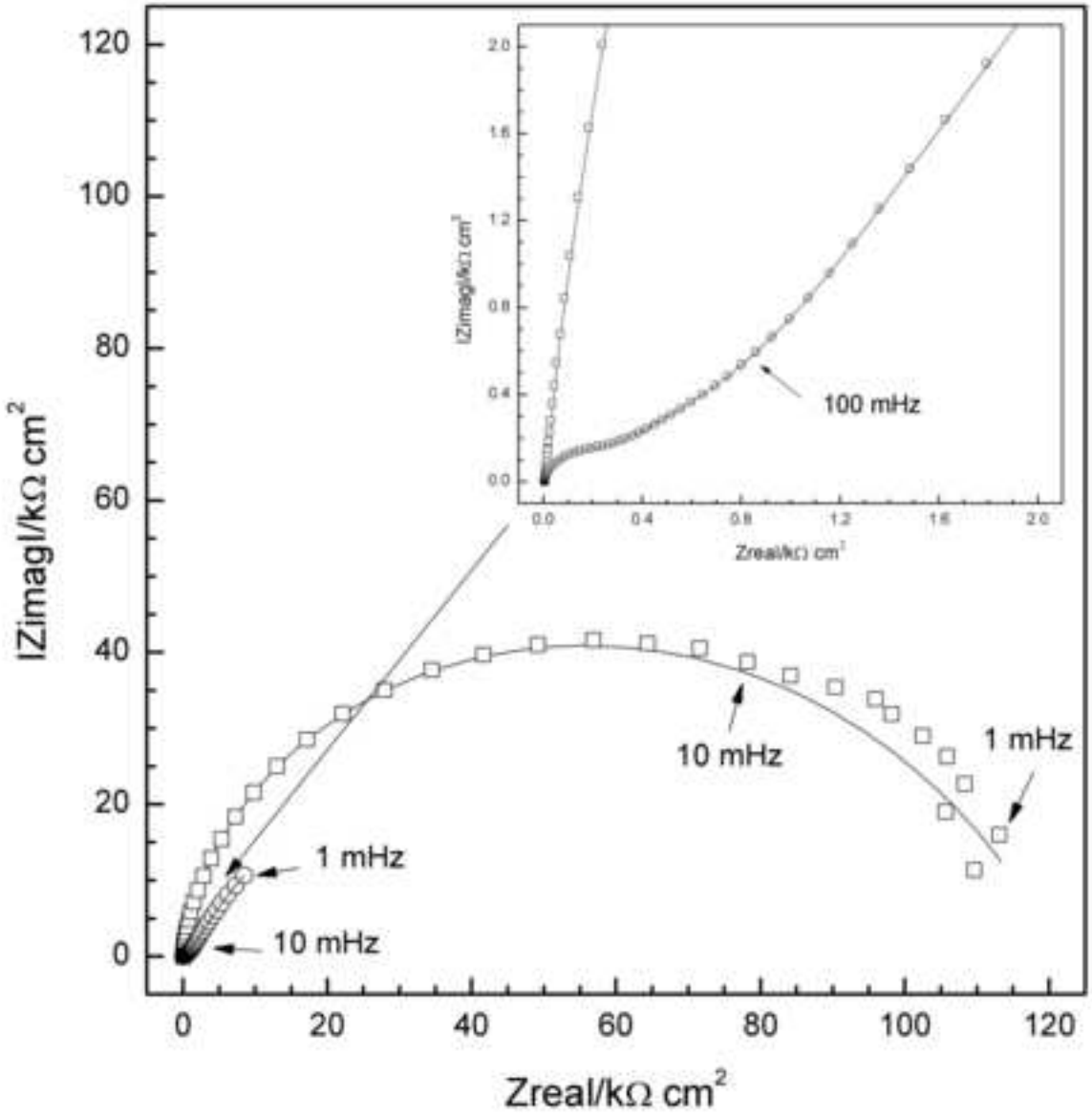

Figure 5b

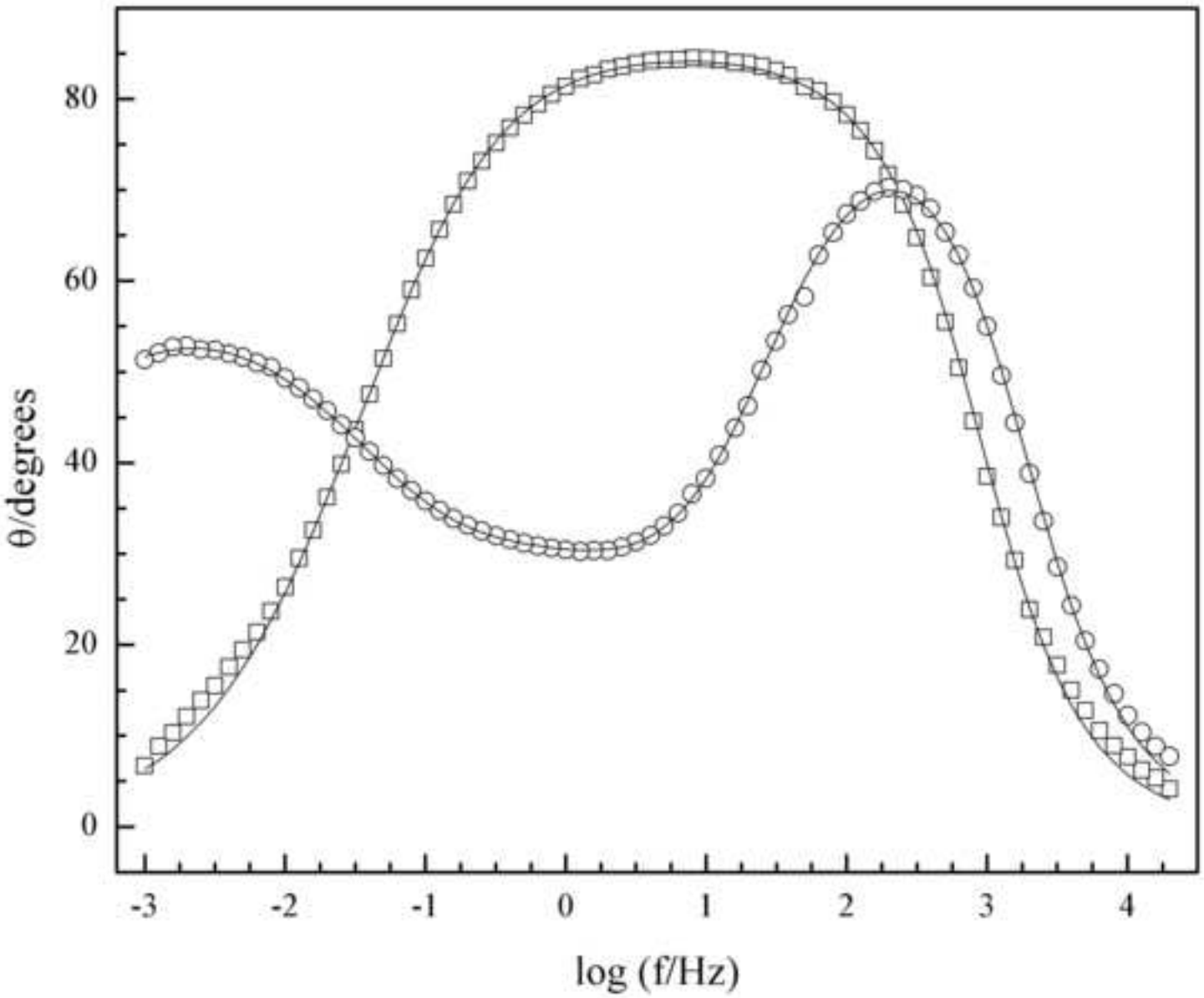

Figure 5c

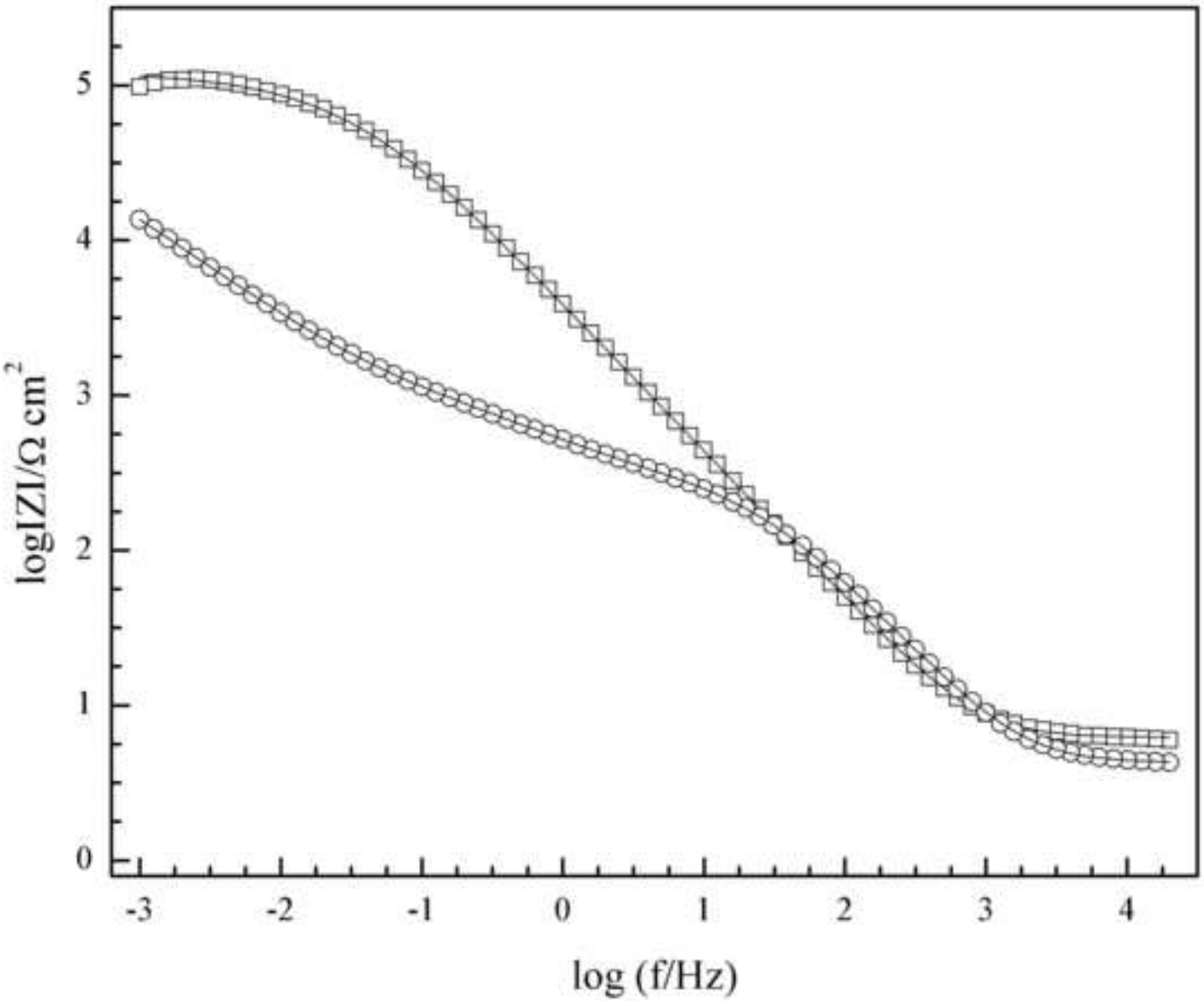

Figure 5d

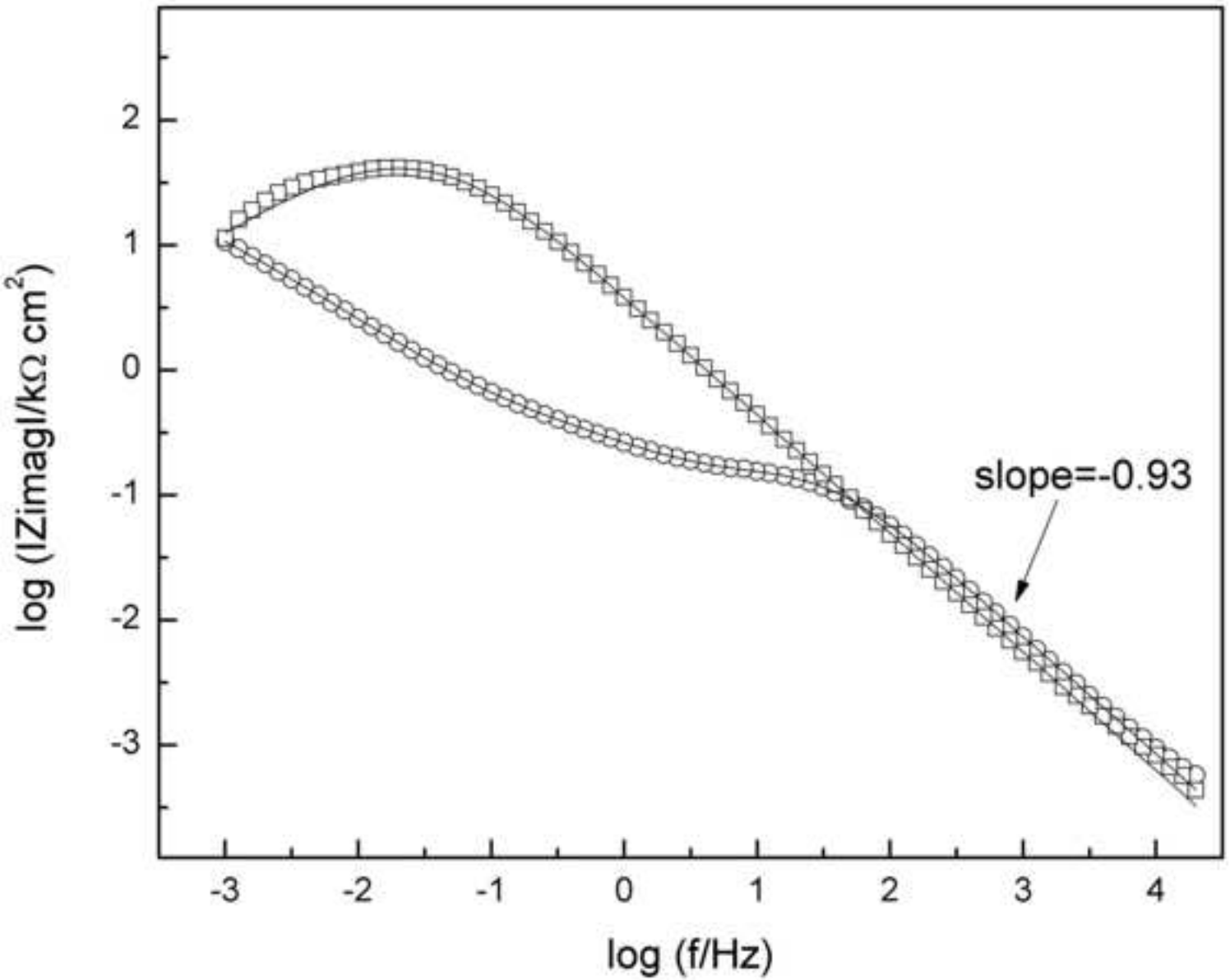

Figure 6

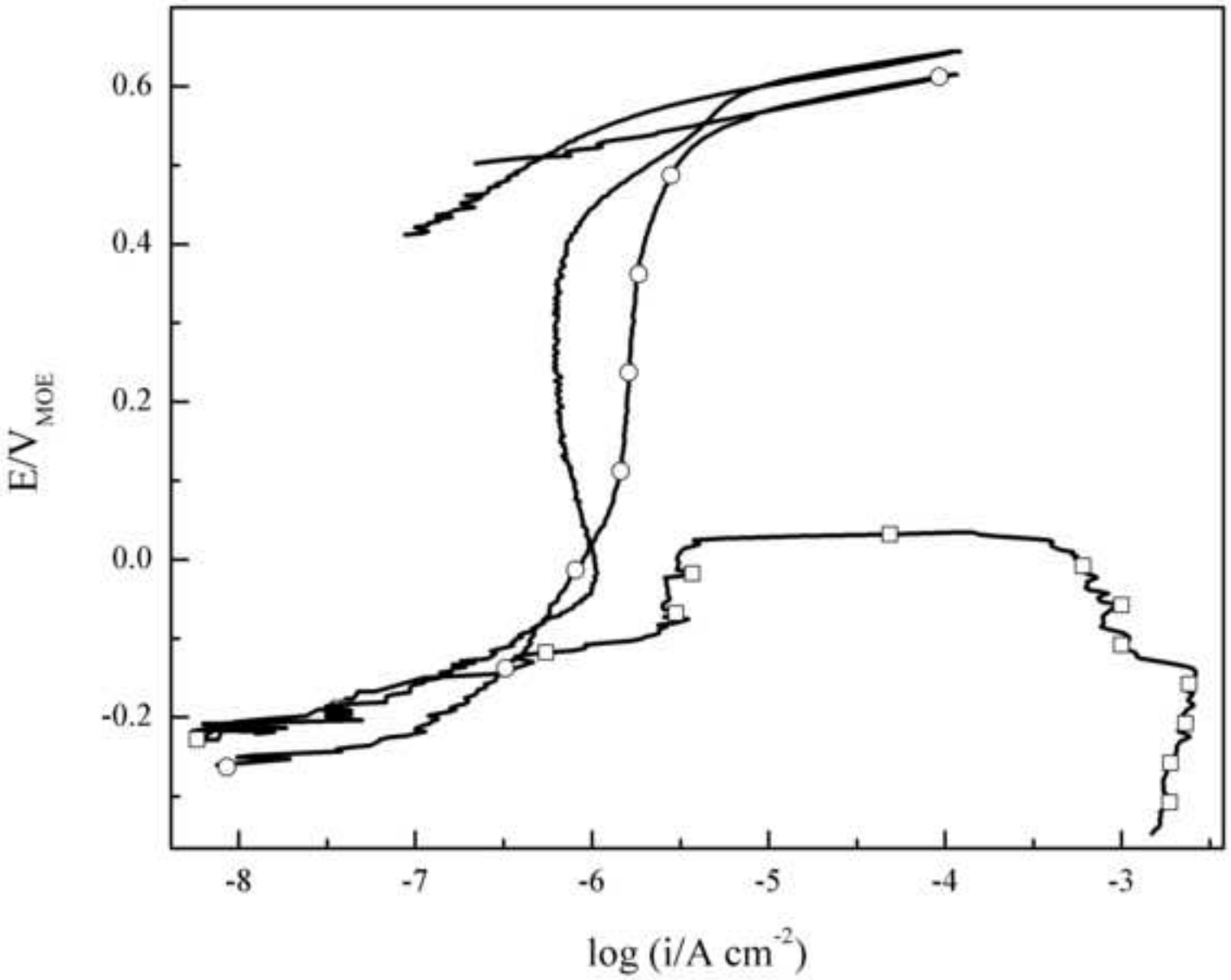

Figure 7

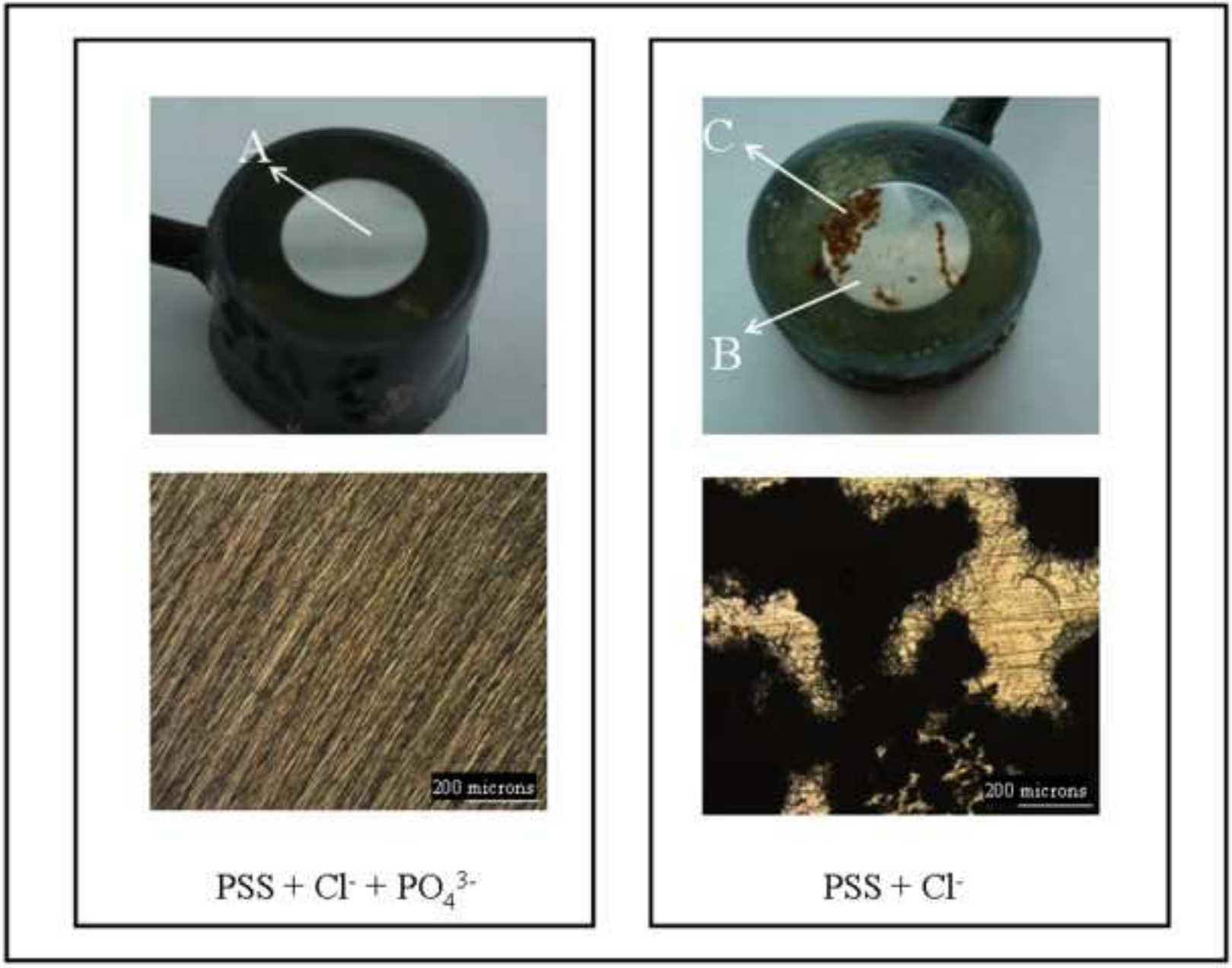

Figure 8

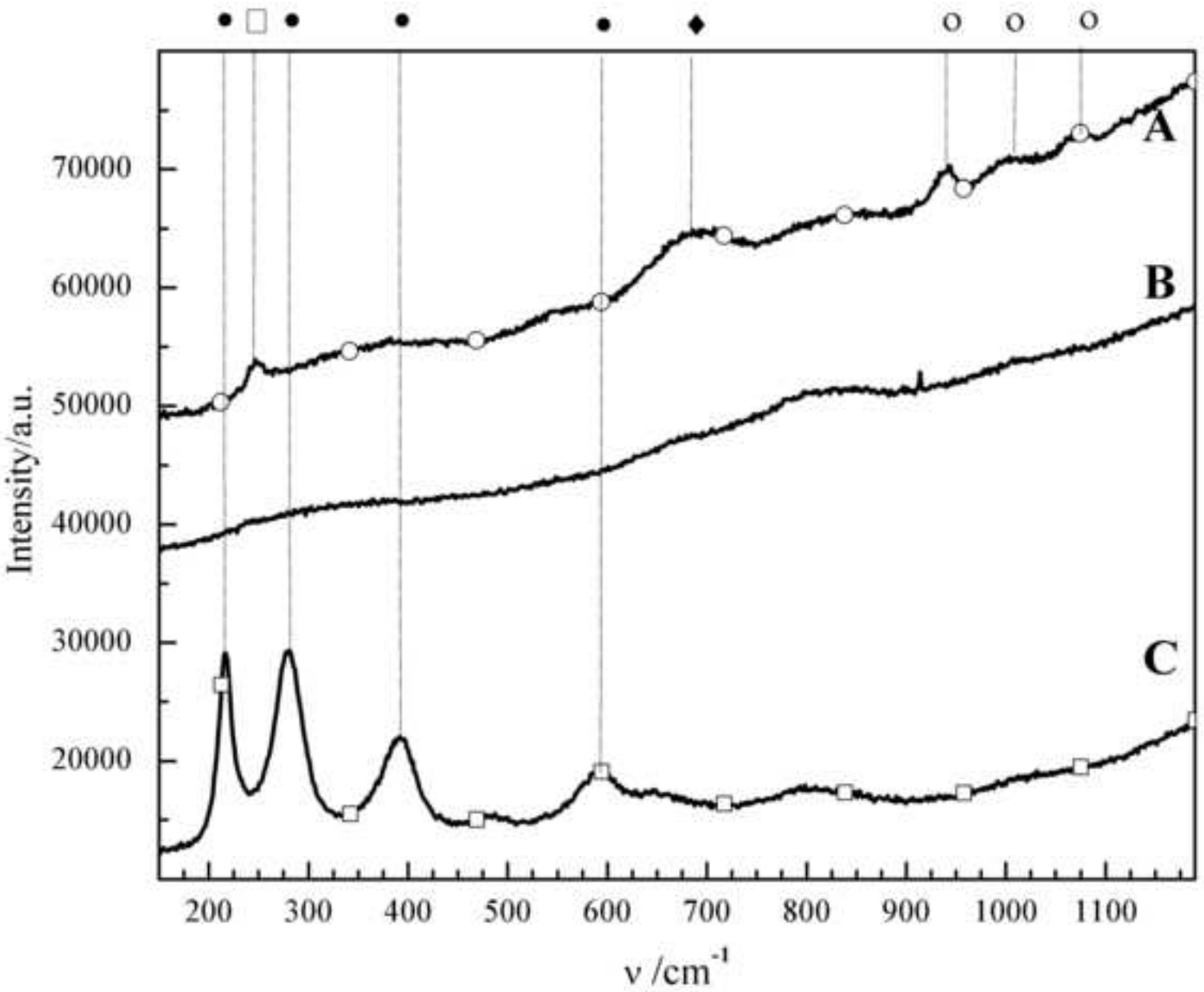
A
B
C
Intensity/a.u.
70000
60000
50000
40000
30000
20000
200
300
400
500
600
700
800
900
1000
1100
ν /cm-1

Figure 9

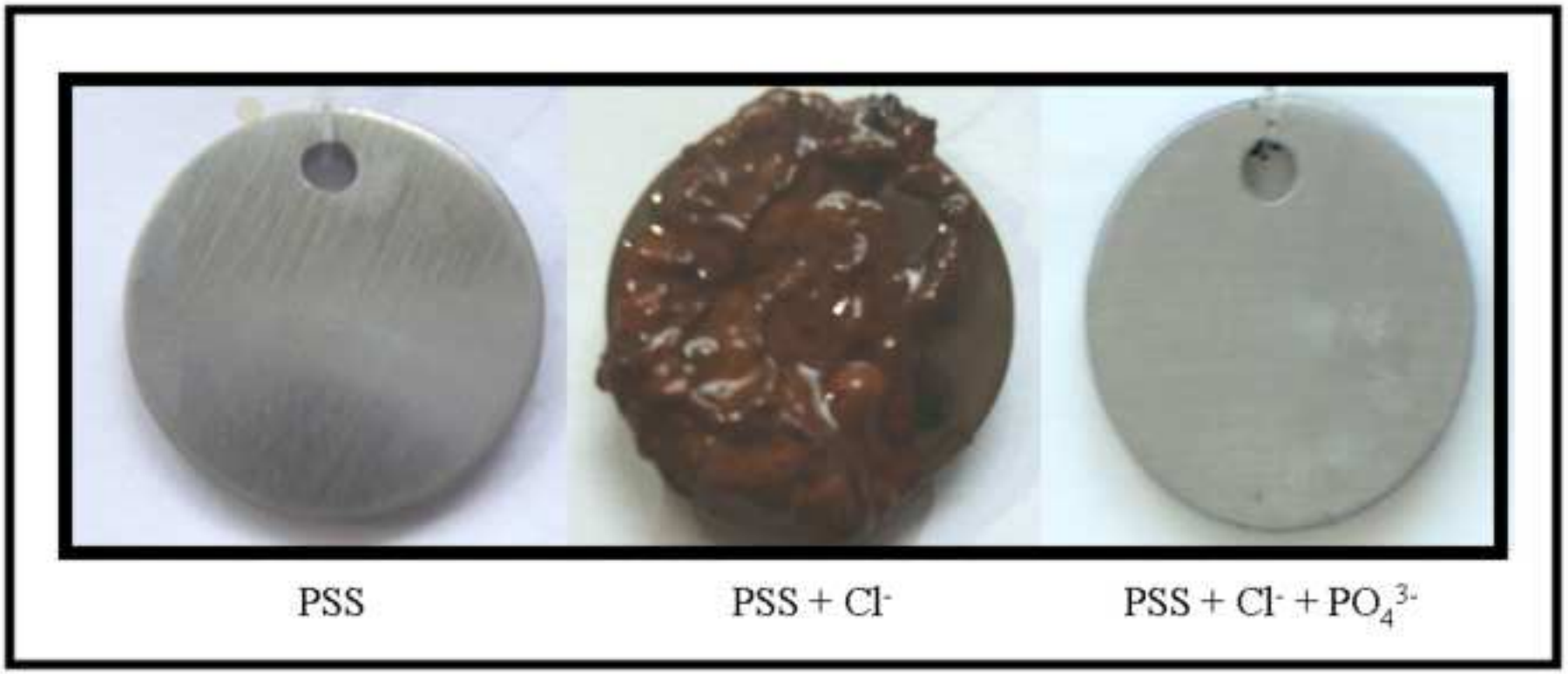

Figure 10

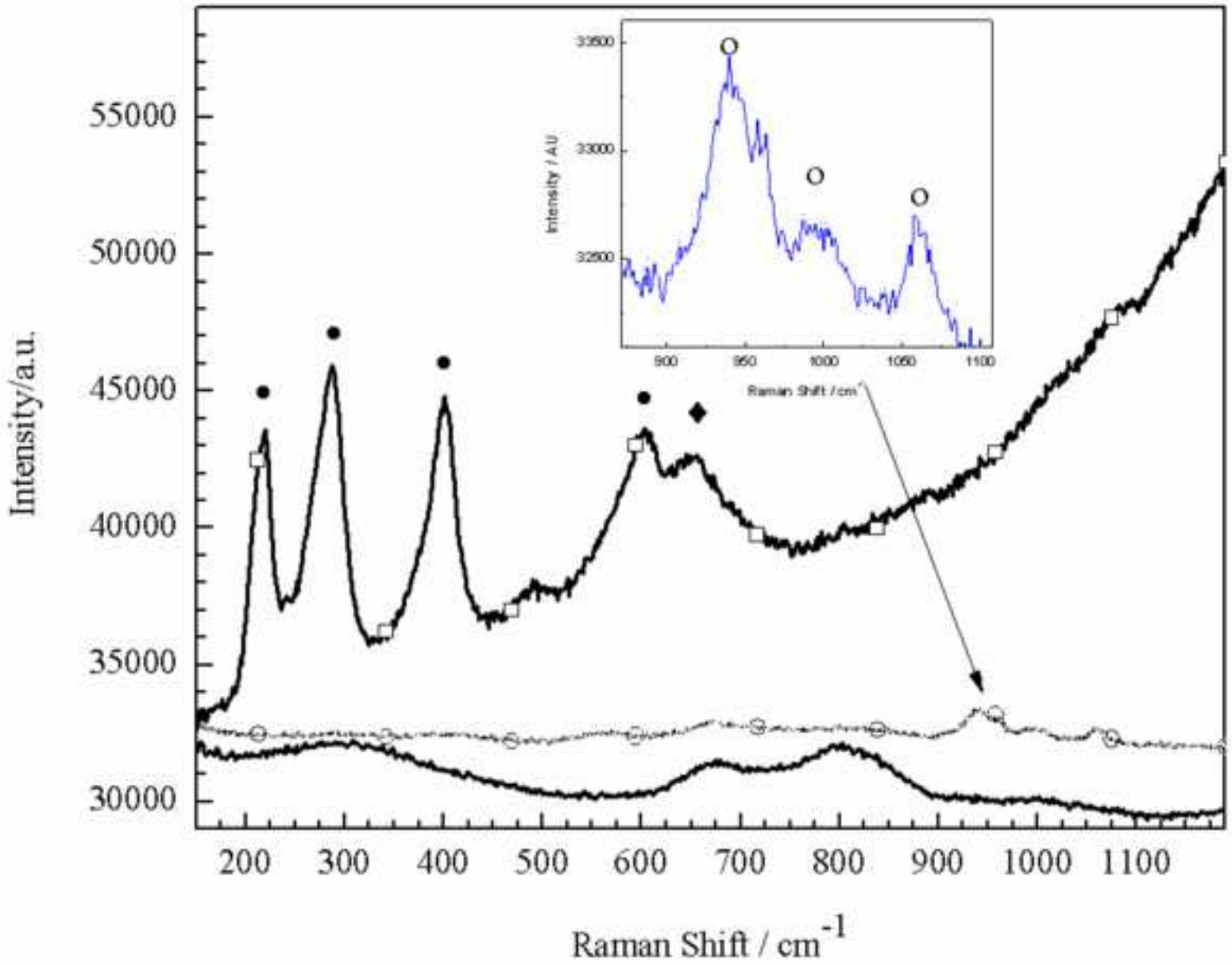
Intensity/a.u.
55000
50000
45000
40000
35000
30000
200
300
400
500
600
700
800
900
1000
1100
Raman Shift / cm-1
Intensity / A.U
3350
3300
3250
900
950
1000
1050
1100
Raman Shift /cm-1